Observed variability of surface layer in the Central Bay of Bengal: results of measurements using glider

Shijo Zacharia[1,2,*], R. Seshasayanan[2], Tata Sudhakar[1], M. A. Atmanand[1] and R. R. Rao[1]

[1]National Institute of Ocean Technology, Ministry of Earth Sciences, Pallikaranai, Chennai 600 100, India
[2]College of Engineering, Guindy Campus, Anna University, Chennai 600 025, India

Underwater gliders measure high-resolution spatio-temporal oceanographic data. In April 2014, the National Institute of Ocean Technology, Chennai operated an underwater glider 'Barathi', for 127 days for observation of Bay of Bengal (BoB). In this article we present the effectiveness of the glider Barathi for high resolution temporal sampling of the surface layer in the central BoB for studying variation of temperature, salinity and density structures and acoustic characteristics on 26–27 May 2014. The results showed 'afternoon effect' on acoustic characteristics and formation of secondary sound channel. Our data set is strongly correlated (coefficient of determination $r^2 > 0.96$) with data from a nearby Array for real-time geostrophic Oceanography (Argo) float.

Keywords: Bay of Bengal, density, eddy, glider, salinity, SLD, MLD, ocean observation, temperature.

IMPROVED ability to observe the Bay of Bengal (BoB) in real time assumes paramount importance in understanding its process. Exhaustive knowledge of upper layer vertical characteristic is beneficial for short-term weather prediction, fisheries and sonar operations. The sonic layer depth (SLD) information is important to understand acoustic properties of the surface duct. It influences acoustic communications[1] and acoustic tomography[2]. The mixed layer depth (MLD) information is crucial in ocean dynamics and climate change studies. Seasonal variability of MLD and SLD over Indian Ocean region were studied earlier[3–12]. But lack of adequate temperature and salinity profiles of the upper ocean hamper our knowledge and understanding of variability of surface layer structure in the BoB[12].

The presence of a research vessel often contaminates near-surface measurements. The temperature profiles collected by small platforms and moored systems show a little stratification in the upper layer, even under low-wind, high insolation conditions[13–15]. The autonomous underwater vehicles (AUV) and free rising profilers measure accurate upper layer information. They are deployed clear of research vessel to minimize vessel-induced errors in measurements. The AUV endurance and spatial coverage are limited to measure physical process of the upper layer[16]. Floats in Array are cost-effective platforms for sampling sub-surface of the ocean[17]. They naturally drift by the ocean current. The buoyancy-driven Argo floats failed to surface when density of float was greater than environmental density[17–19]. The buoyancy-driven underwater vehicles encounter difficulty in BoB due to variations in density and temperature. Hence gliders have not been used to conduct operations in the Indian Ocean[20–22]. The National Institute of Ocean Technology (NIOT), Chennai introduced[23,24] a new *in situ* ocean observation technology, underwater glider in BoB in September 2013.

In this article, we present the effectiveness of glider Barathi for high resolution temporal sampling in the West Central BoB, to study the variation of temperature, salinity and density structure and acoustic characteristics of the surface layer. Our data set on 27 May 2014 was also compared with data from a nearby Argo float.

Materials and methods

Glider

Gliders are unmanned autonomous underwater vehicles with variable buoyancy[25–27]. The NIOT instituted an underwater glider ('Barathi', model: Slocum G2-1000 m, manufactured by Teledyne Webb Research, USA) mission from 24 April to 28 August 2014 in the central BoB[23,24,28]. For a neutrally buoyant underwater glider, increase in volume reduces its density and creates positive buoyancy. Similarly decrease in volume of the glider increases its density and creates negative buoyancy. The buoyancy and attitude results in generation of hydrodynamic lift and drag forces on the wings and body of the glider. A pre-programmed value of buoyancy (±2.6N) and pitch (±26°) for maximum horizontal velocity aids the glider in sliding along vertically and voyage horizontally.

*For correspondence. (e-mail: zacharia@niot.res.in)

Table 1. Specifications of glider Barathi sensors

Sensor	Conductivity (S/m)	Temperature (°C)	Pressure (dbar)
Parameter			
Measurement range	0 to 9°	–5 to +42	0 to 2000
Calibration range	0 to 6°	+1 to +32	Full scale range
Accuracy	±0.0003	±0.002	±0.1% of full scale range
Stability (typical)	0.0003/month	0.0002/month	0.05% of full scale/year
Resolution	0.00001	0.001	0.002% of full scale range

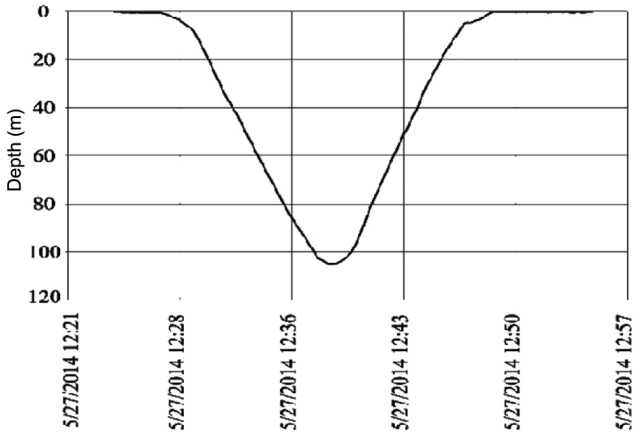

Figure 1. Typical depth profile of the glider Barathi.

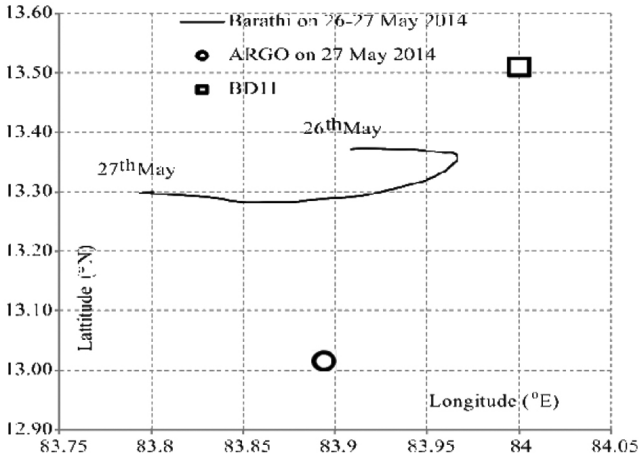

Figure 2. Trajectory of glider Barathi on 26–27 May 2014 (line), position of Argo float on 27 May 2014 (circle), position of data buoy (BD11) (box).

Data

The glider Barathi was equipped with conductivity sensor, temperature sensor, pressure sensor (Table 1) and global positioning system (GPS). It was programmed to dive to 100 m depth and climb to surface consecutively on 26–27 May 2014. It measured 56 temperature (T) and conductivity (C) profiles during this period. Further it recorded surface positions from GPS before each dive. In fact the glider took 1860 sec for one dive and climb operation (Figure 1). The science computer was programmed to measure conductivity, temperature and depth at once in every one meter during down cast. The T and C profile data from the glider was averaged with bin size of 2 m depth. They were then linearly interpolated to standard depths at 2 m.

Study area

The glider Barathi operated with 100 m dive depth in and around the position 13.3°N 83.9°E on 26–27 May 2014. The glider voyaged about 30 km (Figure 2) during the period.

Sea surface height and sea surface temperature

Data archiving, validation, and interpretation of satellite oceanographic (AVISO) altimetry data provided global data at a spatial resolution of 0.25° sea surface height and 0.5° for geo-strophic currents[29].

The sea surface temperature (SST) on 26–27 May 2014 over the study area from advanced very high resolution radiometer (AVHRR) data archive was analysed to investigate physical environment to infer results[30]. The AVHRR data set has 4 km spatial resolution and 14 times a day temporal resolution.

Array for Argo float

A vertical profile of temperature and salinity from Argo float[31–33] (No. 5904334, cycle No. 042) on 27 May 2014 at 13.015°N 83.874°E (Figure 2) was compared with the glider data. The Argo float was away by 33 km towards south from the glider on that day. The data from the ARGO float was linearly interpolated to 2 m resolution in the range of 2–100 m depth.

Air temperature, wave height and wind speed

The air temperature, wave height and wind speed data on 26–27 May 2014 from moored data buoy (BD11)[34,35] at 13.51°N, 84.00°E (Figure 2) were analysed to interpret results. The glider was within 18–33 km range from BD11 during the study period.

Sonic layer depth

The salinity and sound speed profiles were computed from conductivity, temperature and pressure data measured by the glider[36]. Sonic layer depth (SLD) for each profile was computed as near-surface first maximum in sound speed profile (SSP)[9,12,37,38].

The surface duct was bound above by the sea surface and below by SLD[39]. The sound rays refracted and reflected alternately within the surface duct. The sound wave attenuation in the surface duct was much less than normal spherical spreading. The maximum wave length (λ_{max}) of sound wave trapped in the surface duct zone was estimated as[37]

$$\lambda_{max} = 8.51 \times 10^{-3} H^{3/2}, \quad (1)$$

where H is the width (depth) of the surface duct.

Assuming that sound speed is 1500 m/s, the minimum cut-off frequency (f_{min}) of the surface duct was computed by

$$f_{min} = 1.76 \times 10^{5} H^{-3/2}. \quad (2)$$

Mixed layer depth

MLD is defined[10,11,40] as the depth at which the density is greater than the surface by 0.125 kg m^{-3}. The wave action agitates the water near the surface, forming a mixed

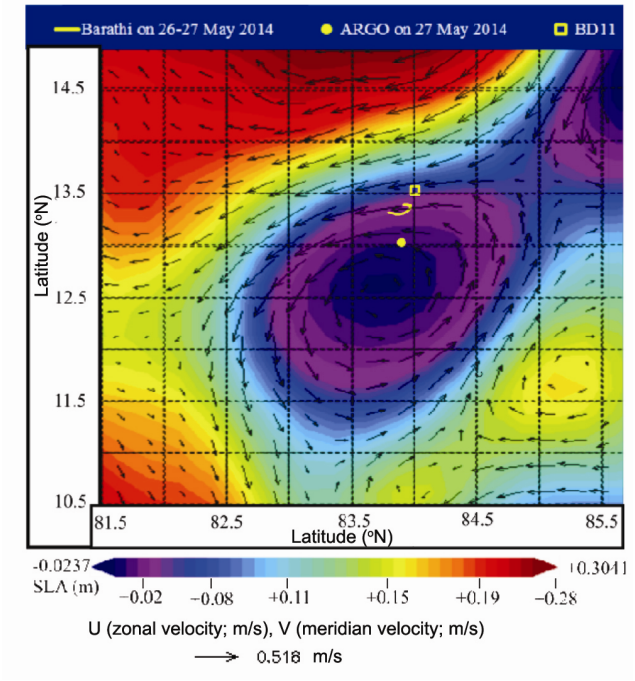

Figure 3. Maps of SLA and absolute sea surface geostrophic velocity from AVISO on 27 May 2014, trajectory of glider Barathi on 26–27 May 2014 (line), Position of data buoy (BD11) on 26–27 May 2014 (box), Possition of argo on 27 May 2014 (circle).

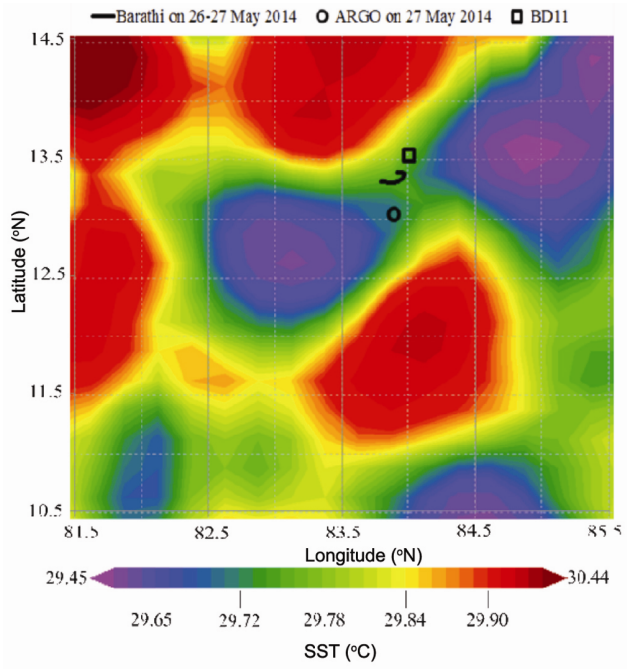

Figure 4. SST on 27 May 2014 from AVHRR, Trajectory of glider Barathi on 26–27 May 2014 (line), Position of data buoy (BD11) on 26–27 May 2014 (box), Position of Argo on 27 May 2014 (circle).

Table 2. Mean and SD of the temperature and salinity profiles

Variable profile name	Temperature (°C)		Salinity (PSS-78)	
	Mean	SD	Mean	SD
Glider	27.788	1.857	33.410	0.667
Argo	27.748	2.1991	33.326	0.818

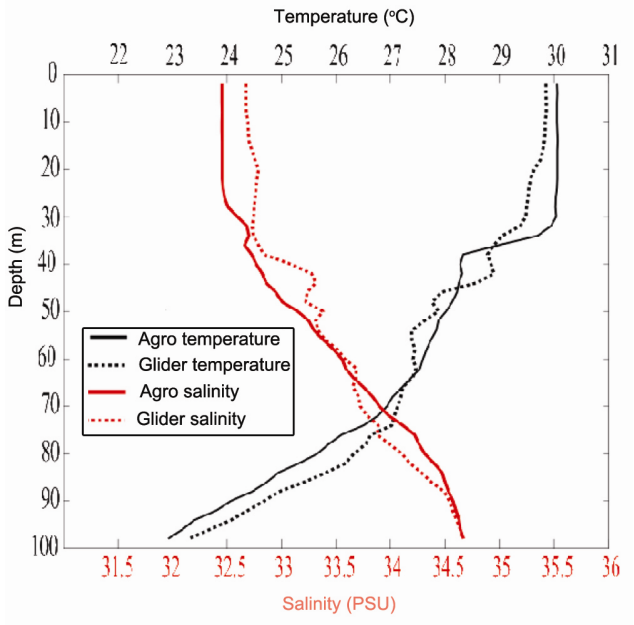

Figure 5. Typical vertical profiles of temperature and salinity measured by glider Barathi and Argo float on 27 May 2014.

layer. Density is calculated from the interpolated temperature, pressure and conductivity data[36].

Results and discussion

Physical environment

The map of sea level anomaly (SLA; Figure 3) from AVISO on 27 May 2014 shows a counter clockwise movement of water in the study area[41,42]. The weak eddy was centred at 12.6°N, 83.7°E. The absolute geostrophic velocity of 0.3–0.5 m/s (Figure 3) was noticed from AVISO for the period in the region of measurement. Even though the glider was commanded towards east with way point, it drifted away in south-west direction since the geostrophic velocity was more than maximum horizontal speed (0.25 m/s) of the glider.

The SST anomaly (Figure 4) analysed on 27 May 2014 from AVHRR was less than 1°C in the region. The distance between core of the eddy and the glider, the data buoy and the Argo float were 78 km, 105 km, 48 km respectively.

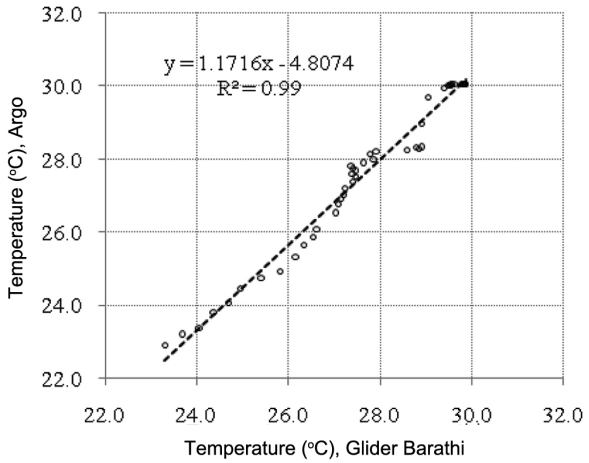

Figure 6. Scatter plot of temperature profiles of glider Barathi and Argo.

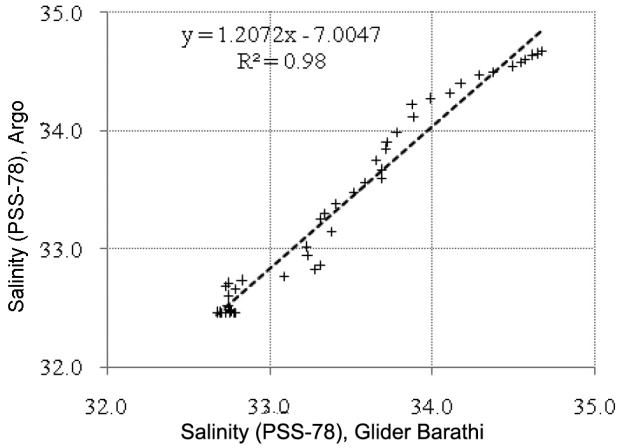

Figure 7. Scatter plot of salinity profiles of glider Barathi and Argo.

Comparisons of Barathi data with the Argo float data

The glider measured temperature (T) and conductivity (C) depth profiles up to 100 m depth. The salinity (S) profile is computed from the temperature, conductivity and depth data set[36]. The temperature and salinity data from glider and ARGO float were linearly interpolated with 2 m resolution in the range of 2–100 m depth. The vertical profiles of temperature and salinity measured by glider (14 : 39 : 33 h on 27 May 2014) and Argo (22 : 49 : 58 h on 27 May 2014) were compared (Figure 5). The mean and standard deviation (SD) of the T and S profiles are shown in Table 2. The root mean square deviation (RMSD) of temperature (0.448°C) and salinity (0.213 PSS78) profiles of the glider and Argo were computed. The temperature (Figure 6) and salinity (Figure 7) profiles were strongly correlated with coefficient of determination r^2 values of 0.99 and 0.98 respectively. Near the sea surface, the glider recorded cooler temperature (–0.199°C) and higher salinity (+0.221PSS78) than Argo. The salinity and temperature measurements coincided at 54 m and 80 m depth respectively. Thereafter the glider recorded marginally warm sub-surface water masses with low salinity. The absolute maximum differences in the measured temperature and salinity were 0.853°C (at 82 m depth) and 0.453 PSS78 (at 42 m depth) respectively. These discrepancies are due to spatial and temporal differences of the measurements. Similar differences were also seen in Barathi data set.

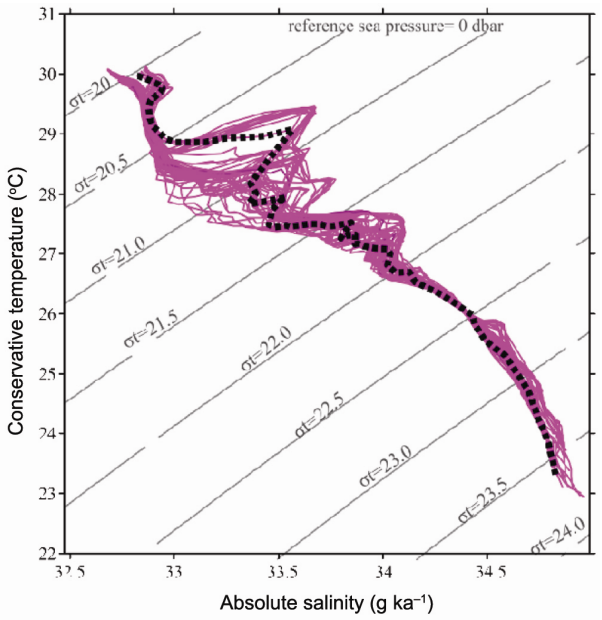

Figure 8. T–S diagram, with density as sigma-t, of the 56 profiles (magenta), average T–S diagram (black dots).

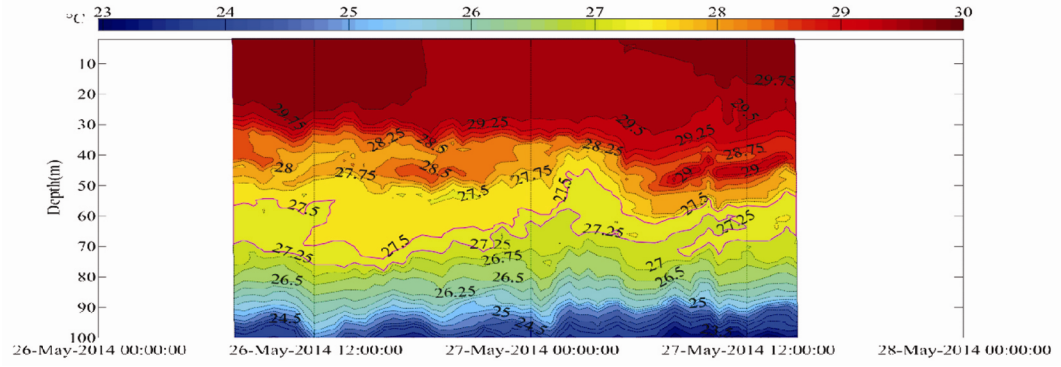

Figure 9. Depth-time section of temperature (contour intervals are 0.25°C), temperature contour of 27.5°C (magenta line).

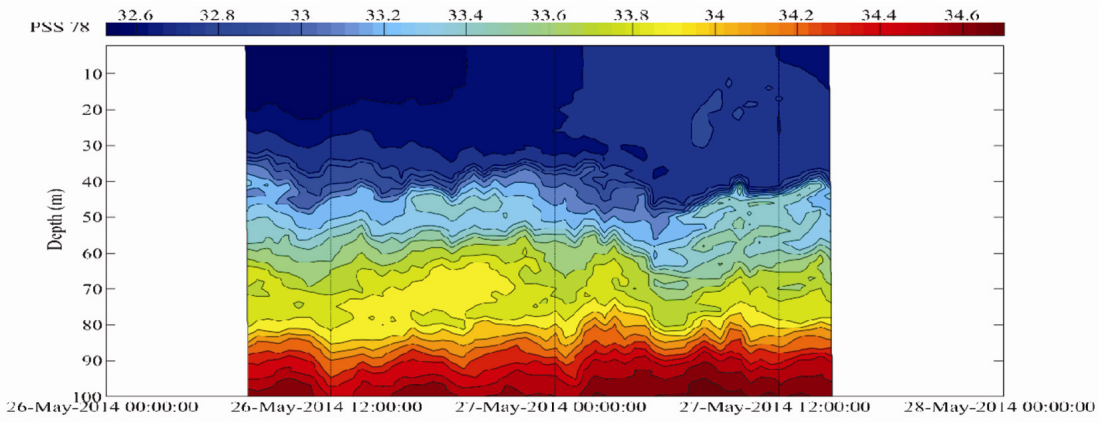

Figure 10. Depth-time section of salinity (contour intervals are 0.1PSS78).

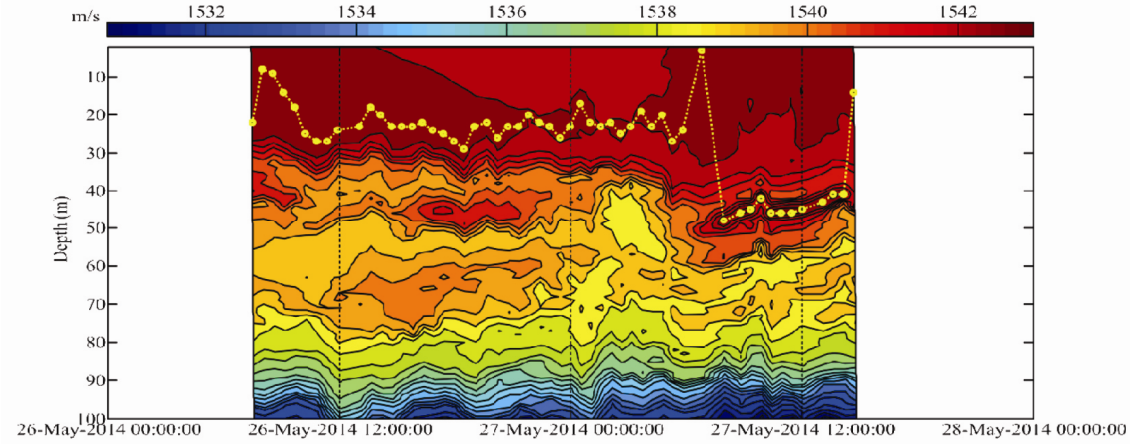

Figure 11. Depth-time section of sound speed (Contour intervals are 0.5 m/s) and SLD (dotted yellow line).

Temperature and salinity structure

The salinity (*S*) profiles were computed from the temperature, conductivity and depth data set[36]. The temperature–salinity (*T*–*S*) diagrams (Figure 8) were computed from the measured data set. All the profiles had low salinity warm water near surface and high saline cold water deeper. The surface layer ranges beyond 100 m depth with low saline water (31–34.7PSS-78). These water properties resemble the BoB water[43,44].

Sub-surface warm water masses were seen at 40–60 m depth in depth-time sections of temperature (Figure 9) in the afternoons to early morning. It was seen that the sub-surface warm water masses had 0.25–0.50°C higher

temperature. The 28°C isotherm shoaled from 50 m on 26 May 2014 to 38 m on 27 May 2014. A similar upwelling was noticed in 28–26°C isotherms. The vertical thermal sections showed troughs and ridges in the isothermal patterns[45]. The temperature of upper 30 m water column decreased by 0.25°C on early hours on 27 May 2014 due to enhanced mixing in the upper ocean for the period[46,47]. The warm water masses in the subsurface layer were traceable with salinity of 33.4–33.5 PSS78 in depth-time sections of salinity (Figure 10). The oscillations in above parameters were seen even at 90 m depth during the observation period.

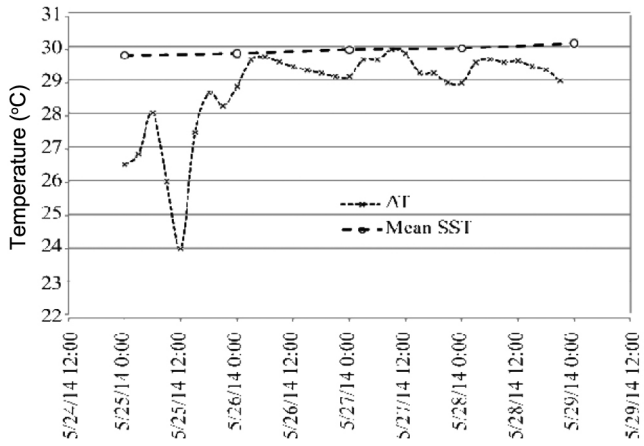

Figure 12. Time series of air temperature (AT) from BD11 and daily mean SST (mean SST) from AVHRR.

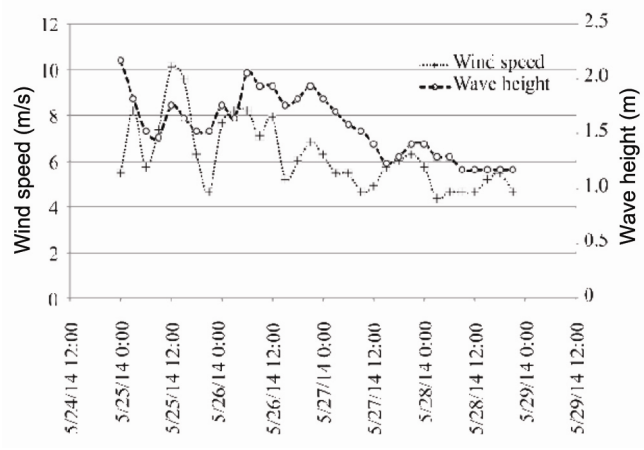

Figure 13. Time series of wind speed and wave height from BD11 on 24–29 May 2014.

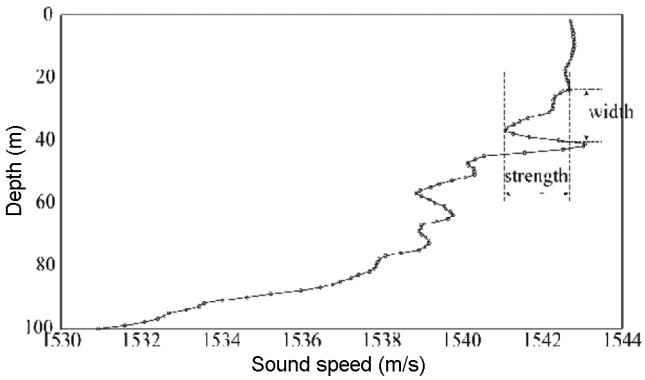

Figure 14. A typical sound speed profile with secondary sound channel at 12 : 23 : 55 h on 27 May 2014.

Acoustic characteristics of the surface layer

The sound speed profiles were computed from *T*, *S* and depth data[36]. The depth-time section of sound speed (Figure 11) on 26–27 May 2014 showed large variations in sound speed in the mixed layer. A sub-surface sound speed (1539 m/s) minimum was noticed at 40–58 m depth from 1 : 30–4 : 30 h on 27 May 2014. The SLD (Figure 11, Table 3) was computed from sound speed profiles. It was seen that SLD was thinned to 3 m at 06 : 49 h on 27 May 2014 due to 'afternoon effect'[48,49]. The air temperature (Figure 12), wave height (Figure 13) and wind speed (Figure 13) from BD11 and daily mean SST from AVHRR (Figure 12) showed that 27 May 2014 was a calm and sunny day. The sub-surface warm water mass deepened the SLD to 42–48 m from 07 : 49 on 27 May 2014. The cooler surface layer water masses and warmer

Table 3. Statistical parameters of SLD

Parameter	Value (m)
Minimum	3
Maximum	48
Mean	26.17
Standard deviation	10.49

Table 4. Statistical parameters of MLD

MLD parameter	Value (m)
Minimum	9
Maximum	27
Mean	19.76
Standard deviation	5.065

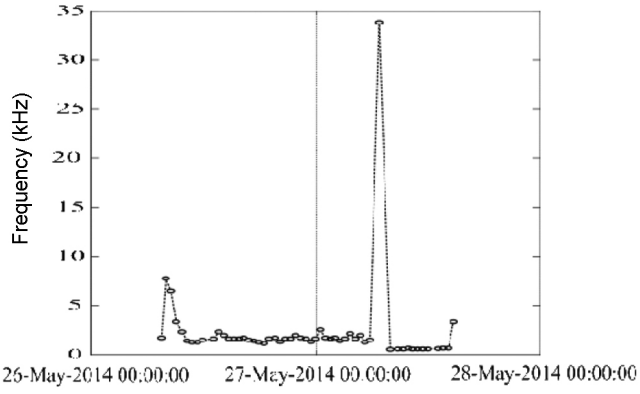

Figure 15. Temporal variation of lower cut-off frequency of the surface duct.

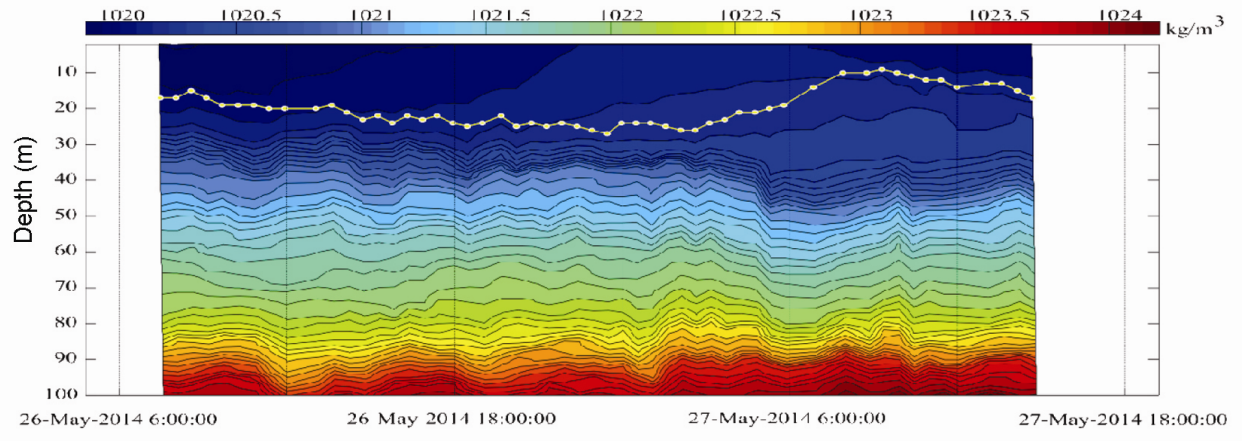

Figure 16. Depth-time section of density (contour intervals are 0.125 kg m^{-3}) and MLD (yellow line).

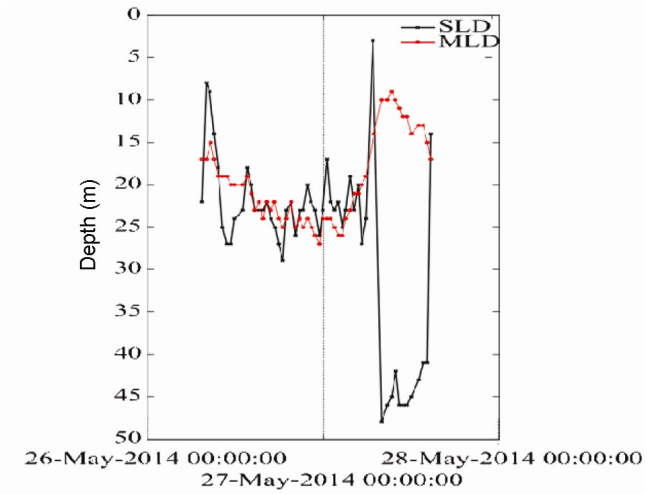

Figure 17. Time series of SLD and MLD.

sub-surface water masses formed a discernable transient weak secondary sound channel (SSC)[50]. The temperature inversion created a deep sound speed maximum on 27 May 2014. A sound speed profile in this region (Figure 14, 12 : 23 h on 27 May 2014) showed SSC channel with axis at 37 m depth. It was characterized with 1.6041 m/s change in sound speed (strength) and 17 m channel depth (width). It was seen that, the sub-surface peak of sound speed (1543.0996 m/s) was higher than near surface (1542.7360 m/s). The presence of eddies in the region justified the transitory nature of SSC.

The temporal variation of lower cut-off frequency (Figure 15) of the surface duct is was calculated according to eq. (2). The lower cut-off frequency was increased to 33.87 kHz when the SLD thinned to 3 m.

Density structure

The density profile (Figure 16) was calculated from the temperature, salinity and pressure data set. All these profiles have stable buoyancy. MLD (Figure 16, Table 4) was computed from density profiles.

Density and sound speed responded differently to depth gradients of temperature and salinity. The sub-surface warm water masses created maximum deep, sound, speed and deepened the SLD than MLD[51] (Figure 17).

Conclusions

In this study we have presented the effectiveness of glider Barathi for high resolution temporal sampling in the west central BoB. A total of 56 temperature and conductivity profiles measured on 26–27 May 2014 were analysed. The map of SLA and absolute geostrophic velocity from AVISO and SST anomaly from AVHRR showed a counter clockwise movement of water in the study area. It was centred at about 12.6°N, 83.7°E. The temperature ($r^2 = 0.96$) and salinity ($r^2 = 0.97$) profiles of the glider and the Argo float were strongly correlated. The *T*–*S* diagrams of all the profiles resembled to indicate the BoB water. Sub-surface warm water masses were found at 40–60 m depth in depth-time sections of temperature in the afternoons to early morning. The warm water masses in the sub-surface layer are traceable with salinity of 33.4–33.5 PSS78. Upwelling of 28–26°C isotherms was seen during the period. The temperature of upper 30 m water column was decreased by 0.25°C in the early hours on 27 May 2014 due to enhanced mixing in the upper ocean for the period. A sub-surface sound speed (1539 m/s) minimum was noticed at 40–58 m depth from 1 : 30–4 : 30 h on 27 May 2014. It was seen that SLD was thinned to 3 m at 06 : 49 h on 27 May 2014 due to 'afternoon effect' on a calm and sunny day. The cooler surface layer water masses and warmer sub-surface water masses formed discernable transient weak SSC. The sub-surface peak of sound speed (1543.0996 m/s) was higher than near surface (1542.7360 m/s). The lower cut-off frequency of the surface duct was increased to 33.87 kHz when the SLD

thinned to 3 m. All these profiles had stable buoyancy. The sub-surface warm water masses created deep sound speed maximum and deepened the SLD than MLD.

Concurrent samplings with multiple gliders as function of space and time are needed to understand spatial and temporal variability of the ocean.

1. Siderius, M., Porter, M. B., Hurskey, P., McDonald, V. and the KauaiEx Group, Effects of ocean thermocline variability on non-coherent underwater acoustic communications, *J. Acoust. Soc. Am.*, 2007, **121**, 1895–1908.
2. Sutton, P. J., Worcester, P. F., Masters, G., Cornuelle, B. D. and Lynch, J. F., Ocean mixed layers and acoustic pulse propagation in the Greenland Sea. *J. Acoust. Soc. Am.*, 1993, **94**, 1517–1526.
3. Hareesh Kumar, P. V., The sound channel characteristics in the south central Bay of Bengal. *Int. J. Innov. Technol. Exp. Eng.*, ISSN: 2278-3075, 2013, **3**(6), 61–65.
4. Prasannakumar, S., Murty, T. V. R., Somayajulu, Y. K., Chodankar, P. V. and Murty, C. S., Reference sound speed profile and related ray acoustics of Bay of Bengal for tomographic studies. *Acta Acustica*, 1994, **80**, 127–137.
5. Prasannakumar, S., Somayajulu, Y. K. and Murty, T. V. R., Acoustic propagation characteristics and tomography studies of the northern Indian Ocean, In *Acoustic Remote Sensing Applications* (ed. Singal, S. P.), Narosa, New Delhi, 1997, pp. 551–581.
6. Murty, T. V. R., Somayajulu, Y. K. and Sastry, J. S., Computations of some acoustic ray parameters in the Bay of Bengal. *Indian J. Mar. Sci.*, 1990, **19**, 235–245.
7. Murty, T. V. R., Somayajulu, Y. K. and Sastry, Simulation of acoustic propagation along a section in the western Bay of Bengal. *J. Pure Appl. Ultra*., 1990, **12**, 29–33.
8. Murty, T. V. R. *et al.*, Objective mapping of observed sub-surface mesoscale cold core eddy in the Bay of Bengal by stochastic inverse technique with tomographically simulated travel times. *Indian J. Geo. Mar. Sci.*, 2011, **40**, 307–324.
9. Udaya Bhaskar, T. V. S., Debadatta Swain and Ravichandran, M., Sonic layer depth variability in the Arabian Sea. *Int. J. Oceans Oceanogr*., 2010, **4**, 17–28.
10. Udaya Bhaskar, T. V. S., Swain, D., Ravichandran, M., Inferring mixed-layer depth variability from Argo observation in the western Indian Ocean. *J. Mar. Res.*, 2006, **64**, 393–406.
11. Udaya Bhaskar, T. V. S., Swain, D. and Ravichandran, M., Mixed layer variability in the Northern Arabian Sea as detected by an Argo float. *Ocean Sci. J.*, 2007, **42**(4), 241–246.
12. Udaya Bhaskar, T. V. S., Swain, D. and Ravichandran, M., Seasonal variability of Sonic Layer depth in the central Arabian Sea. *Ocean Sci. J.*, 2008, **43**(3), 147–152.
13. Farrar, J. T., Zappa, C. J., Weller, R. A. and Jessup, A. T., Sea surface temperature signatures of oceanic internal waves in low winds. *J. Geophys. Res. Oceans*, 2007, **112**, C06014.
14. Walsh, E. J. *et al.*, Coupling of internal waves on the main thermocline to the diurnal surface layer and sea surface temperature during the tropical Ocean – global atmosphere coupled ocean–atmosphere response experiment. *J. Geophys. Res.*, 1998, **103**, 12,612–12,628.
15. Benjamin, A., Hodges and David M. Fratantoni, AUV observations of the diurnal surface layer in the north Atlantic salinity maximum. *J. Phys. Oceanogr*., 2014, **44**, 1595–1604; doi:http://dx.doi.org/10.1175/JPO-D-13-0140.1.
16. http://auvac.org/explore-database/browse-database (accessed on 8 August 2014).
17. Ravichandran, P. N.. Vinayachandran, Sudheer Joseph and Radhakrishnan, K., Results from first ARGO float deployed by India. *Curr. Sci.*, 2004, **86**(5), 651–659.
18. http://www.jamstec.go.jp/ARGO/argo_web/results/system_building/deployment/weight_adjustment/TR-ballasting2.pdf (accessed on 1 May 2015).
19. Kobayahi, T. *et al.*, Quality control of Argo data based on high quality climatological data set (HydroBase) I, http://www.jamstec.go.jp/ARGO/argo_web/results/data_management/management/quality_control_1/Quality_control.pdf (accessed on 19 January 2015).
20. http://www.ioos.noaa.gov/observing/observing_assets/glider_asset_map.html (accessed on 6th February 2015).
21. http://marine.rutgers.edu/cool/auvs/ (accessed on 6 February 2015).
22. http://www.incois.gov.in/portal/datainfo/insituhome.jsp (accessed on 6 February 2015).
23. Shijo Zacharia, *et al.*, Glider operations in the Bay of Bengal. In proceedings of IEEE International Symposium on Underwater Technology, Chennai, India, 2015; doi: 10.1109/UT.2015.7108279.
24. Shijo Zacharia, *et al.*, Initial set of oceanographic data from Bay of Bengal by means of an underwater glider as mobile sensor node. *Curr. Sci.*, 2015, **109**(5), 918–928.
25. Stommel, H., The Slocum mission. *Oceanography*, 1989, **l**(2), 22–25.
26. Bachmayer, R., Leonard, N. E., Graver, J., Fiorelli, E., Battha, P. and Palley, D., Underwater gliders: recent developments and future applications. In proceedings of the IEEE International Symposium on Underwater Technology. Taipei, Taiwan, 2004.
27. Rudnick, D. L., Davis, R. E., Eriksen, C. C., Fratantoni, D. M. and Perry, M. J., Underwater gliders for ocean research. *Mar. Tech. Soc. J.*, 2004, **38**, 73–84; doi:10.4031/002533204787522703.
28. http://www.webbresearch.com/pdf/Slocum_Glider_Data_Sheet.pdf (accessed on 6 February 2015).
29. http://las.aviso.oceanobs.com/las/getUI.do (accessed on 6 February 2015).
30. http://las.incois.gov.in/ (accessed on 6 February 2015).
31. http://www.argo.ucsd.edu/Argo_GE.html (accessed on 6 February 2015).
32. Oka, E. Ando, K., Stability of temperature and conductivity sensors of Argo profiling floats. *J. Oceanogr.*, 2004, **60**, 253–258.
33. http://ftp.seabird.com/products/spec_sheets/41data.html (accessed on 6 February 2015).
34. http://www.incois.gov.in/portal/datainfo/mooredpositions.html (accessed on 6 February 2015).
35. Venkatesan, R. *et al.*, In situ ocean subsurface time-series measurements from OMNI buoy network in the Bay of Bengal. *Curr. Sci.*, 2013, **104**(9), 1166–1177.
36. Fofonoff, P. and Millard Jr, R. C., Algorithms for computation of fundamental properties of seawater. *Unesco Tech. Pap. Mar. Sci.*, 1983, **44**, 46–49.
37. Etter, C. P., Underwater Acoustic Modelling: Principles, Techniques and Applications. E&FN Spon, London, 2nd edn, 1996, p. 88.
38. Jain, S., Ali, M. M. and Sen, P. N., Estimation of sonic layer depth from surface parameters. *Geophys. Res. Lett.*, 2007, **34**, L17602; doi:10.1029/2007GL030577.
39. Urick, R. J., Principles of underwater sound. McGraw-Hill, New York, USA, 1983, 3rd edn, p. 423.
40. Ohno, Y., Kobayashi, T., Iwasaka, N. and Suga, T., The mixed layer depth in the North Pacific as detected by the Argo floats. *Geophys. Res. Lett.*, 2004, **31**, L11306; doi:10.1029/2004GL019576.
41. McGillicuddy Jr, D. J., Johnson, R., Siegel, D. A., Michaels, A. F., Bates, N. R. and Knap, A. H., Mesoscale variations of biochemical properties in the Sargasso Sea. *J. Geophys. Res.*, 1999, **104**(C6), 13381–13394; http://dx.doi.org/10.1029/1999JC900021.
42. Hwang, C., Wu, C. R. and Kao, R., TOPEX/poseidon observations of mesoscale eddies over the subtropical countercurrent: kinematic characteristics of an anticyclonic eddy and a cyclonic eddy. *J. Geophys. Res*., 2004, **109**, C08013; doi:10.1029/2003JC002026.

43. Tomczak, M. and Godfrey, J. S., Regional Oceanography: An Introduction, 2001, Chapter 12, http://www.es.flinders.edu.au/~mattom/regoc/pdffiles/colour/single/12P-Indian.pdf (accessed on 6 February 2015).
44. http://www.incois.gov.in/Images/iogoos/abstracts/abstract1.htm (accessed on 6 February 2015).
45. Gopalan, A. K. S., Gopala Krishna, V. V., Ali, M. M. and Sharma Rashmi, Detection of Bay of Bengal eddies from TOPEX and in situ observations. *J. Mar. Res*., 2000, **58**, 721–734.
46. Isern-Fontanet, J., Garcia-Ladona, E. and Font, J., Vortices of the mediterranean sea: an altimetric perspective. *J. Phys. Oceanogr*., 2006, **36**, 87–103.
47. Hu, J., Gan, J., Sun, Z., Zhu, J. and Dai, M., Observed three-dimensional structure of a cold eddy in the southwestern South China Sea. *J. Geophys. Res*., 2011, **116**, C05016; doi:10.1029/2010JC006810.
48. Richard, P., Hodges, Underwater Acoustics Analysis, Design and Performance of SONAR. John Wiley & Sons, Ltd, New Delhi, India, 2010, p. 227.
49. Lowrence E. Kinsler, Austin R. Frey, Alan B. Coppens, James V. Sanders, Fundamentals of Acoustics, John Wiley & Sons, Inc, New York, USA, 2000, 4th edn, p. 440.
50. Chow, R. K. and Browning, D. G., A study of secondary sound channels due to temperature inversions in the Northeast Pacific Ocean. *J. Acoust. Soc. Am*., 1982, **72**, S57; http://dx.doi.org/10.1121/1.2019957.
51. Robert, W. H., Barron, C. N., Cames, M. R. and Zingareli, R. A., Evaluating the sonic layer depth relative to the mixed layer depth. *J. Geophys. Res*., 2008, **113**, C07033; doi:10.1029/2007/JC004595.

ACKNOWLEDGEMENTS. We acknowledge the Ministry of Earth Sciences, Government of India for funding this research and the Vessel Management Group, NIOT for providing the ship. We acknowledge the active support of Mr G. Suresh and the Ocean Electronic Department, NIOT for deployment operations. We are grateful to the Teledyne Webb Research Corporation, USA, for the glider and technical support and the National Center for Atmospheric Research Staff, USA, for easy access to AVISO data. We also thank Indian National Centre for Ocean Information Services (INCOIS) Hyderabad, for providing data from buoy, AVHRR and Argo data service in Live Access Server.

Received 2 September 2015; revised accepted 16 June 2017

doi: 10.18520/cs/v113/i11/2151-2159